Chemical Science

Accepted Manuscript

This article can be cited before page numbers have been issued, to do this please use: X. Shi, X. Chen, Y. Huang, Z. Liu, B. Zhao, L. Yan, T. Zhang, H. Fu and L. Wang, *Chem. Sci.*, 2026, DOI: 10.1039/D5SC06978E.

ROYAL SOCIETY OF CHEMISTRY

rsc.li/chemical-science

View Article Online
DOI: 10.1039/D5SC06978E

EDGE ARTICLE

Efficient singlet fission in rubicene null aggregates

Xiaomei Shi,*[a] Xinyu Chen,[b] Yu Huang,[c] Zuyuan Liu,[b] Bo Zhao,[b] Lingpeng Yan,[b] Teng-Shuo Zhang,*[c] Hongbing Fu[d] and Long Wang*[b]

0Received 00th January 20xx,
Accepted 00th January 20xx

DOI: 10.1039/x0xx00000x

The singlet fission (SF) photovoltaic applications are currently restricted by the limited number of practical SF materials and the underlying SF mechanism in typical molecular aggregates. Null-aggregates are molecular aggregates that exhibit minimal exciton-exciton interactions leading to a monomer-like spectroscopic signature and thus hold some different advantages to bypass extra energy loss and excimer trap issues in conventional H- and J-aggregates. However, it remains unknown if null-aggregates could also contribute to an efficient SF process. In this work, we presented an efficient SF system based on rubicene null aggregates. The comprehensive structural and spectroscopic studies demonstrate that the destructive interference between long-range Coulomb and short-range charge-transfer (CT) couplings lead to the monomer-like absorption characteristics of the null aggregates. More importantly, the siginicant CT coupling interactions contribute to an efficient SF process with a SF rate of $(1.0\ ps)^{-1}$ and a triplet yield of 192% in the null aggregates. Our findings not only provide a deep insight into the SF mechanism in the special null aggregates but also offer a robust SF material system with suitable energies, which would open up new avenue for the future molecular design and device applications.

Introduction

Singlet fission (SF) that transforms one excited singlet into two triplets has gathered extensive attention owing to its potential in alleviating the thermalization losses and substantially enhance conversion efficiency of solar cells.[1-7] Recently, the range of SF materials continues to grow, and such MEG process has been found in a series of small molecules, oligomers, and conjugated polymers.[8-17] Encouragingly, the implementation of the SF-based devices with the external quantum efficiency over 100% represented huge milestone and further arose extensive research interests.[5] However, a highly efficient SF molecular system integration into real photovoltaic applications remains to be discovered. As a general rule, SF candidates must fulfill the basic energetic requirement that the excitation energy of singlet, $E(S_1)$, closes to twice that of triplet state, $2E(T_1)$.[1, 2] Besides, these materials demand for suitable intermolecular interactions to deliver efficient multiexciton generation.[1, 2] This generally requires the delicate adjusting and engineering of molecular orientation and film morphology in the solid aggregates. Moreover, excessive molecular aggregation might greatly reduce singlet energy not only limiting the efficient coversion of high-energy photons but also leading to an over-endothermic SF energetics resulting in the loss of SF. Therefore, aside from basic material design, gaining indepth understanding on the underlying SF mechanism in typical molecular aggregates is still a challenging but urgent work.

Molecular exciton theory describes that the staggered "head-to-tail" molecular arrangement forms J-aggregate exhibiting red-shifted absorption signature, while the cofacial "side-by-side" packing generate H-aggregate featuring blue-shifted absorption characteristic (Scheme 1).[18] In recent years, there are many theoretical and experimental studies on the influences of H- and/or J-aggregate on SF dynamics.[12, 19-27] Nevertheless, the excessive J-type aggregation might greatly reduce singlet energy leading to not only extra energy loss but also an over-endothermic SF energetics to slow or even stop SF process, while the strong coupled H-type aggregation might usually form an excimer trap state detrimental to energy conversion process. Null-aggregates, as the name suggests, are molecular aggregates that exhibit minimal exciton-exciton interactions leading to a monomer-like spectroscopic signature in the condensed state.[28-32] Thus, such molecular aggregates hold some different advantages, which might provide an alternative to the aforementioned extra energy loss and excimer trap issues in the conventional aggregates. Recently, Hong et al. reported efficient multiexciton generation in dilute solution of a null exciton-coupled perylenediimide folda-dimer.[33] However, it remains unknown if null aggregates could also contribute to an efficient SF process. In this work, we presented an efficient SF system based on rubicene (tRc) null aggregates (Scheme 1). The comprehensive structural and spectroscopic measurements suggest that the destructive interference between long-range Coulomb coupling and short-range charge-transfer (CT) coupling lead to the monomer-like

[a] Department of Biochemistry and Molecular Biology, Shanxi Medical University, Taiyuan 030001, P. R. China. Email: shxm@sxmu.edu.cn
[b] Key Laboratory of Interface Science and Engineering in Advanced Materials, Ministry of Education, Taiyuan University of Technology, Taiyuan 030024, P. R. China. Email: wanglong@tyut.edu.cn
[c] College of Chemical Engineering, Zhejiang University of Technology, Hangzhou, Zhejiang 310014, P. R. China. Email: zhangts@zjut.edu.cn
[d] Beijing Key Laboratory for Optical Materials and Photonic Devices, Department of Chemistry, Capital Normal University, Beijing 100048, P. R. China.
Electronic Supplementary Information (ESI) available: [details of any supplementary information available should be included here]. See DOI: 10.1039/x0xx00000x

absorption characteristics of the current tRc null aggregates. More importantly, strong CT coupling interactions contribute to an efficient SF process with a SF rate, k_{SF}, of (1.0 ± 0.2 ps)$^{-1}$ and a triplet yield (TY) of 192 ± 30% in the null aggregates. Our findings not only provide a highlight the SF mechanism in the special null aggregates but also offer a robust SF material system, which are important considerations in the future molecular design and device applications.

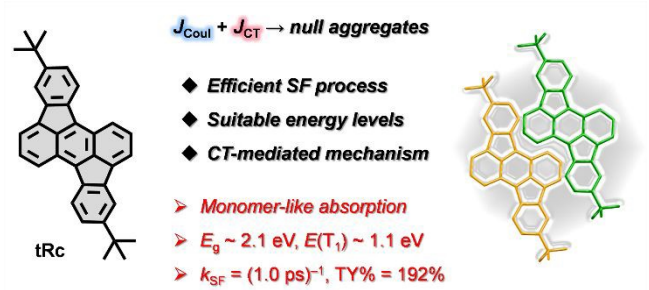

Scheme 1. Efficient SF system based on rubicene (tRc) null aggregates.

Results and discussion

Steady state characterizations.

The polycyclic conjugated hydrocarbon rubicene skeleton viewed as a C70 fullerene fragment has recently garnered broad synthetic and optoelectronic application interests.[34-40] In the previous work, we have employed structural aromaticity to modulate the basic photophysical properties of optoelectronic materials, and designed a new SF material based on rubicene skeleton with efficient SF process, and excellent stability.[33] In this work, we designed the *tert*-butyl-substituted rubicene derivative, tRc, in order to further optimize the SF properties and elucidate the underlying SF mechanism in the solid aggregates. The compound was synthesized using the previously reported method (see the section 2 of the Supporting Information).

Firstly, we conducted steady-state characterizations for tRc molecules in the dilute solution and vapor-deposited thin films (Figure 1). Figure 1a displays the UV/vis absorption and photoluminescence (PL) spectra. In monomer state, the molecules show the blue-green absorption peaks at 476, 509 and 540 nm, and the strong orange emission at 580 nm with a fluorescence lifetime of 4.52 ± 0.01 ns (Figure 1b). In the thin films, the X-ray diffraction (XRD) measurements confirm that they are polycrystalline in nature and exhibit a preferred orientation with the (100) plane parallel to the substrate (Figure 1c). Fascinatingly, the line shapes of the absorption spectra of the thin films closely match those of monomeric tRc suggesting null exciton coupling in the condensed state (Figure 1a).[28] The optical band gap (E_g) is estimated to be 2.1 eV, which is determined by the intersection wavelength of the absorption and PL spectra of the thin films. A red-edge absorption characteristic is observed around 600 nm, which could be related to the tail states in a polycrystalline film. These results clearly suggest that tRc films turn out to be null aggregates with monomer-like absorption characteristics.

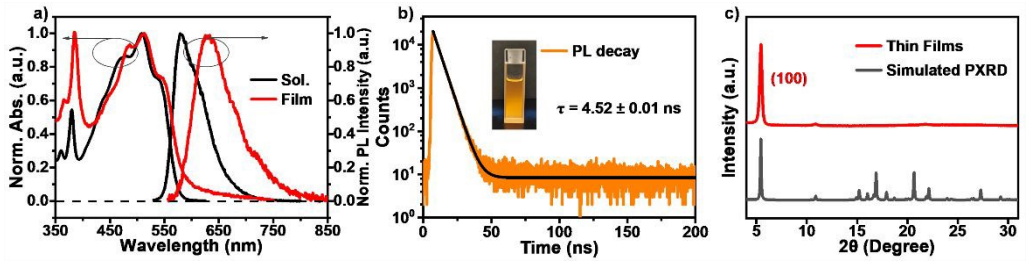

Fig. 1 Steady state characterizations. a) Normalized UV/vis absorption and PL spectra of tRc molecules in dilute CH_2Cl_2 solution (10^{-5} M) and thin films. b) The PL decay curves of tRc molecule in dilute solution (510 nm excitation). c) XRD diffractogram of tRc thin films (red) and simulated powder pattern (black).

Subsequently, we investigated the molecular stacking behaviors of the studied tRc system in the solid state. The single crystal data display that tRc molecules are arranged in a distinct slip stacking pattern with the π-π distance of 3.42 Å and the transverse and longitudinal slip distances of 3.69 and 3.30 Å and slip angles of 46° and 43°, respectively (Figure 2). To further reveal the nature of the null aggregates, we performed theoretical analysis for exciton coupling interactions in the adjacent molecular dimer unit from the crystal data of tRc molecule (for calculation details see the section 4 of the Supporting Information).[28] The results display that tRc dimer system exhibits a relative slip angle of 69° between transition dipole moments (Figure 3). Such an inter-tRc geometry contributes to a positive long-range Coulomb coupling of J_{Coul} = 391 cm^{-1} and a negative CT-mediated short-range coupling of J_{CT} = −195 cm^{-1}. That is, the destructive interference between Coulomb coupling and CT coupling lead to the monomer-like absorption characteristics in the current tRc null aggregates.[28, 33] The theoretical results also reflect that tRc molecule possesses a suitable SF energetics given the singlet and triplet excitation energies, $E(S_1)$ = 2.30 eV and $E(T_1)$ = 1.05 eV, respectively. It should be noted that fluorescence quenching in these null aggregates indicate an ultrafast nonradiative transition outcompetes and dominates the excited state deactivation process.[42-44] These interesting phenomena arouse our curiosity about the excited state photophysics and especially SF possibility for the current tRc null aggregates.

View Article Online
DOI: 10.1039/D5SC06978F

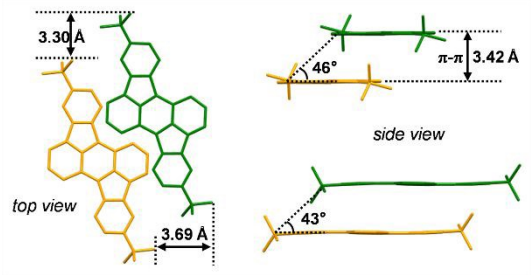

Fig. 2 Molecular stacking arrangements in tRc crystal structures.

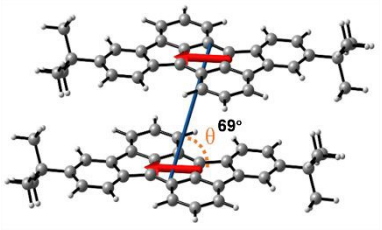

Fig. 3 The transition dipole moment of tRc molecule and the relative slip angle between transition dipole moments of adjacent dimer unit from the crystal data.

Excited state dynamics in dilute solution.

Then we applied femtosecond transient absorption (fsTA) measurements to reveal excited-state deactivation process for tRc molecule in dilute solution (Figure 4). As shown in Figure 4a, the fsTA spectra from dilution solution display the negative signals consisting of ground state bleaching (GSB) and stimulated emission (SE) signals in the 480-650 nm range, and the positive excited state absorption (ESA) bands around 650-800 nm. The line shapes of the spectra remain relatively constant over a period of 6.0 ns indicating that no obvious excited state conversion happens and singlet decay channel dominate the excited state deactivation process. The ESA kinetic at 700 nm decays with two exponentials of τ_1 = 148 ± 19 ps and τ_2 = 4.0 ± 0.2 ns (Figure 4b), which are assigned to the minor excited-state structure adjustment and radiative transition processes, respectively. These results clearly depict that the tRc molecule holds a common fluorescence emission behaviour in a monomer excited state.

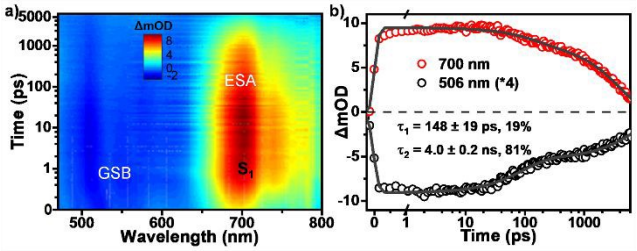

Fig. 4 Excited state decay dynamics in tRc dilute solution. a) Pseudocolor plot and b) kinetic decay curves from fsTA measurements of tRc in dilute solution (450 nm excitation).

Robust SF process in null aggregates.

We then performed TA measurements for the vapor-deposited films to track the excited state deactivation processes and explore the SF possibility in the studied tRc null aggregates (Figure 5). The measurements were carried out at a low excitation fluence of 50 μJ/cm² and the to excitation density dependence tests indicated that TA data were free of the heating and annihilation effects of excitation light (Figure S8). After photo-excitation, the initial fsTA spectra was composed of the negative GSB signals around 470-560 nm and the positive ESA bands around 560-800 nm, which was assigned to the optically populated S_1 state (Figure 5a and 5b). Compared to the solution spectral characteristics (Figure 5a), the TA data show not only similar ESA signal around 700 nm but also two strong ESA peaks at 750 and 775 nm, which was attributed to the absorption signature of CT state. Then concurrent with the rapid attenuation of singlet ESA signals, new ESA bands formed between 470-560 nm, seriously overlapping with the GSB signals, and led to substantial cancellation of overall TA signals. The total changes of the spectral line shapes indicate the formation of new transient species within 80 ps. Then the new species persisted beyond the 6.0 ns detection time window of our fs-TA apparatus. Using parallel samples, nanosecond TA (nsTA) measurements were performed to track the deactivation of the long-lived transient species (Figure 5c). The TA signals on a time scale of ns-to-μs recovered back to ground line without further evolution. Given the line shapes of these signals in the nsTA spectra overlap well with the fs-TA spectral signature, the dominant end species formed upon photo-excitation are undoubtedly individual triplet excitons. The singlet depletion method was then applied to estimate the triplet yield of the tRc films, giving a value of 192 ± 30% (for calculation details see the section 5.4 of the Supporting Information).[45, 46] Given the ultrafast formation rate and high triplet yield, we conclude that an efficient SF process dominates the excited-state deactivation, leading to the observed long-lived triplet populations in the TA spectra. The SF-generated triplet excitons exhibit a characteristic biexponential decay kinetics (Figure S9). These two distinct triplet decay components were then assigned to i) triplet states undergoing *in situ* triplet-triplet annihilation back in the S_0 with τ_1 = 219 ± 12 ns (63.2%) and ii) triplet states that diffuse before annihilation back in the S_0 with τ_2 = 2441 ±80 ns (36.8%), respectively.[41, 44] These results suggest that in the current null aggregates, an efficient SF process could still happen to populate long-lived triplet excitons via a CT-mediated mechanism.

View Article Online
DOI: 10.1039/D5SC06978E

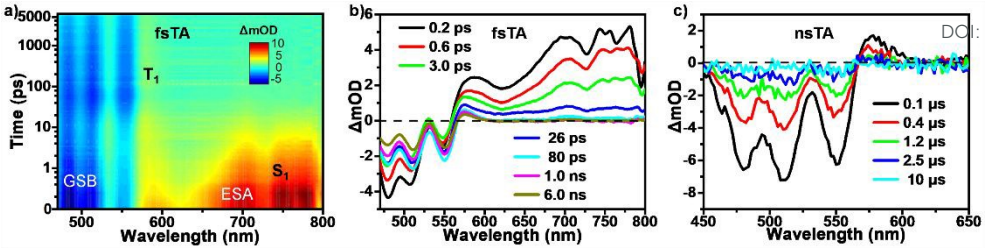

Fig. 5 SF and triplet decay processes in tRc thin films. a) Pseudocolor plot and b) selected spectra for fsTA measurements of tRc thin films (450 nm excitation). c) nsTA spectra from nanosecond laser flash photolysis measurements for tRc thin films (532 nm-excitation, 50 μJ/cm²).

Then we performed global analyses on the fsTA data from tRc thin films (Figure 6). In order to reflect the polycrystalline characteristic of the thin films, we applied a three-state branched kinetic model (Figure 6a). The results show that SF proceeds with two rate constants, k_{SF1} = (1.0 ± 0.2 ps)$^{-1}$ and k_{SF2} = (23 ± 4 ps)$^{-1}$ in the current system (Figure 6b). The SF time scales of the current molecule seem be closer to the endothermic materials like tetracenes and other previous reported SF systems.[10, 14, 15] Based on the optical band gap and theoretical triplet energy, the molecule seems to have an iso-energetic SF event. Since theoretical calculation may underrate triplet state excitation energy, therefore SF is likely to be an endothermic process in the current tRc system. This further reflects the merit of null-aggregates. They exhibits monomer-like absorption characteristics, which could avoid the excessive J-type aggregation that might greatly reduce singlet energy not only leading to the extra energy loss but also resulting in an over-endothermic SF energetics to slow or even stop SF process. That is, a population of the optically populated singlet states nearby hot sites could undergo ultrafast SF with a time constant of (1.0 ± 0.2 ps)$^{-1}$, while the other part of the optically excited singlet excitons that must diffuse to corresponding hot sites and ensue SF with a slightly slower time constant of (23 ± 4 ps)$^{-1}$ (Scheme 2). Subsequently, these SF-formed long-lived triplet excitons could diffuse and persist over several microseconds among polycrystalline films.

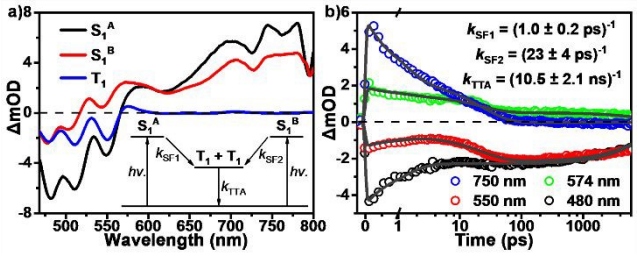

Fig. 6 Global analysis for the fsTA data of tRc films. a) Species-associated spectra and kinetic model. b) Globally fit wavelength kinetics as well as corresponding SF and TTA rate constants.

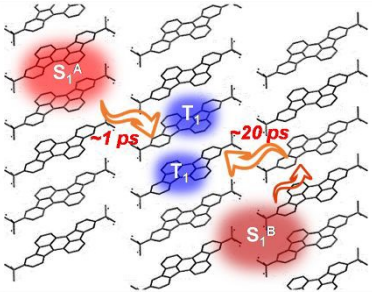

Scheme 2. Schematic diagram of SF processes in the current tRc system.

Discussion.

Based on the aforementioned structural and spectroscopic characteriaztions, we conclude that efficient multiexciton generation processes outcompete other singlet decay pathways of the tRc null aggregate system. Compared to conventional H- and J-aggregate, null aggregate system exhibits monomer-like absorption characteristics. On the one hand, such aggregate pattern could avoid the excessive J-type aggregation that might greatly reduce singlet energy not only leading to the extra energy loss but also resulting in an over-endothermic SF energetics to slow or even stop SF process. On the other hand, it might also skip to form an excimer trap state that usually occurs in the strong coupled H-type aggregate. Our results also demonstrate that the destructive interference between long-range Coulomb and short-range CT coupling lead to the monomer-like absorption characteristics of the current null aggregates. Moreover, the results support a CT-mediated SF mechanism in the null aggregate system. More importantly, the current tRc molecule turns out to be a robust SF material system for enhancing performance of photovoltaic devices given its efficient SF process and suitable enegey levels, including $E(S_1)$ ~2.1 eV and $E(T_1)$ ~1.1 eV.[1, 2]

Conclusions

In summary, an efficient SF system based on rubicene null aggregates was successfully fabricated and investigated. Based on the comprehensive structural and spectroscopic studies, we demonstrate that the destructive interference between long-range Coulomb and short-range CT coupling lead to the monomer-like absorption characteristics of the current null aggregates. More importantly, strong CT coupling interactions contribute to an efficient SF process with a rate of (1.0 ps)$^{-1}$ and a triplet yield of 192% in the null aggregates. Our findings not only provide a deep insight for the SF mechanism in the special

null aggregates but also offer a robust SF material system with suitable energy levels, which are important considerations in the molecular design and device applications.

Author Contributions

X. M. S. and L. W. conceptualized and conceived the project. X. M. S. prepared samples and conducted photophysical characterizations with the assistance of X. Y. C., Z. Y. L., B. Z., L. P. Y., H. B. F. and L. W. H. Y. and T.-S. Z. performed theoretical calculations. X. M. S. and L. W. wrote the manuscript and all the authors participated in the data analysis and discussions.

Conflicts of interest

There are no conflicts to declare.

Acknowledgements

This work was supported by the National Natural Science Foundation of China (Nos. 22501164, 22479107 and 22005210) and by the Fundamental Research Program of Shanxi Province (Nos. 202203021224004 and 20210302124469).

Notes and references

1 M. B. Smith and J. Michl, *Chem. Rev.*, 2010, **110**, 6891-6936.
2 A. Rao and R. H. Friend, *Nat. Rev. Mater.*, 2017, **2**, 17063.
3 K. Miyata, F. S. Conrad-Burton, F. L. Geyer and X. Y. Zhu, *Chem. Rev.*, 2019, **119**, 4261-4292.
4 M. C. Hanna and A. J. Nozik, *J. Appl. Phys.*, 2006, **100**, 074510.
5 D. N. Congreve, J. Y. Lee, N. J. Thompson, E. Hontz, S. R. Yost, P. D. Reusswig, M. E. Bahlke, S. Reineke, T. Van Voorhis and M. A. Baldo, *Science*, 2013, **340**, 334-337.
6 C. A. Nelson, N. R. Monahan and X. Y. Zhu, *Energ. Environ. Sci.*, 2013, **6**, 3508-3519.
7 J. L. Xia, S. N. Sanders, W. Cheng, J. Z. Low, J. P. Liu, L. M. Campos and T. L. Sun, *Adv. Mater.*, 2017, **29**, 1601652.
8 J. C. Johnson, A. J. Nozik and J. Michl, *J. Am. Chem. Soc.*, 2010, **132**, 16302-16303.
9 E. Busby, J. L. Xia, Q. Wu, J. Z. Low, R. Song, J. R. Miller, X. Y. Zhu, L. M. Campos and M. Y. Sfeir, *Nat. Mater.*, 2015, **14**, 426-433.
10 C. M. Mauck, P. E. Hartnett, E. A. Margulies, L. Ma, C. E. Miller, G. C. Schatz, T. J. Marks and M. R. Wasielewski, *J. Am. Chem. Soc.*, 2016, **138**, 11749-11761.
11 J. H. Hu, K. Xu, L. Shen, Q. Wu, G. Y. He, J. Y. Wang, J. Pei, J. L. Xia and M. Y. Sfeir, *Nat. Commun.*, 2018, **9**, 2999.
12 A. K. Le, J. A. Bender, D. H. Arias, D. E. Cotton, J. C. Johnson and S. T. Roberts, *J. Am. Chem. Soc.*, 2018, **140**, 814-826.
13 T. Ullrich, P. Pinter, J. Messelberger, P. Haines, R. Kaur, M. M. Hansmann, D. Munz and D. M. Guldi, *Angew. Chem. Int. Ed.*, 2020, **59**, 7906-7914.
14 L. Wang, L. Lin, J. Yang, Y. Wu, H. Wang, J. Zhu, J. Yao and H. Fu, *J. Am. Chem. Soc.*, 2020, **142**, 10235-10239.
15 L. Wang, X. Shi, S. Feng, W. Liang, H. Fu and J. Yao, *CCS Chem.*, 2022, **4**, 2748-2756.
16 S. Wang, X.-Y. Liu, M. Zhang, L. Wang, G. Cui, H. Fu and J. Yao, *CCS Chem.*, 2024, **6**, 2142-2149.
17 X. Shi, Y. Geng, Z. Wang, E. Zhou, H. Fu and L. Wang, *Adv. Funct. Mater.*, 2025, **35**, 2420771.
18 M. Kasha, H. R. Rawls and M. Ashraf El-Bayoumi, 1965, **11**, 371-392.
19 A. J. Musser, M. Maiuri, D. Brida, G. Cerullo, R. H. Friend and J. Clark, *J. Am. Chem. Soc.*, 2015, **137**, 5130-5139.
20 E. A. Margulies, J. L. Logsdon, C. E. Miller, L. Ma, E. Simonoff, R. M. Young, G. C. Schatz and M. R. Wasielewski, *J. Am. Chem. Soc.*, 2017, **139**, 663-671.
21 H. Zang, Y. Zhao and W. Liang, *J. Phys. Chem. Lett.*, 2017, **8**, 5105-5112.
22 L. Wang, W. Cai, J. Sun, Y. Wu, B. Zhang, X. Tian, S. Guo, W. Liang, H. Fu and J. Yao, *J. Phys. Chem. Lett.*, 2021, **12**, 12276-12282.
23 Y. Kim, M. Han, C. Lee and S. Park, *J. Phys. Chem. B*, 2021, **125**, 7967-7974.
24 A. Kundu and J. Dasgupta, *J. Phys. Chem. Lett.*, 2021, **12**, 1468-1474.
25 A. M. Levine, G. He, G. Bu, P. Ramos, F. Wu, A. Soliman, J. Serrano, D. Pietraru, C. Chan, J. D. Batteas, M. Kowalczyk, S. J. Jang, B. L. Nannenga, M. Y. Sfeir, E. H. R. Tsai and A. B. Braunschweig, *J. Phys. Chem. C*, 2021, **125**, 12207-12213.
26 H. Miyamoto, K. Okada, K. Tokuyama and M. Nakano, *J. Phys. Chem. A*, 2021, **125**, 5585-5600.
27 Z. Wu, J. Duan, X. Chen, X. Tian, X. Shi, H. Fu and L. Wang, *J. Phys. Chem. Lett.*, 2025, **16**, 9273-9279.
28 N. J. Hestand and F. C. Spano, *J. Chem. Phys.*, 2015, **143**, 244707.
29 C. Kaufmann, D. Bialas, M. Stolte and F. Würthner, *J. Am. Chem. Soc.*, 2018, **140**, 9986-9995.
30 E. Sebastian, A. M. Philip, A. Benny and M. Hariharan, *Angew. Chem. Int. Ed.*, 2018, **57**, 15696-15701.
31 M. P. Lijina, A. Benny, R. Ramakrishnan, N. G. Nair and M. Hariharan, *J. Am. Chem. Soc.*, 2020, **142**, 17393-17402.
32 Y. Bo, P. Hou, J. Wan, H. Cao, Y. Liu, L. Xie and D. M. Guldi, *Adv. Mater.*, 2023, **35**, 2302664.
33 Y. Hong, J. Kim, W. Kim, C. Kaufmann, H. Kim, F. Würthner and D. Kim, *J. Am. Chem. Soc.*, 2020, **142**, 7845-7857.
34 H. Lee, Y. Zhang, L. Zhang, T. Mirabito, E. K. Burnett, S. Trahan, A. R. Mohebbi, S. C. B. Mannsfeld, F. Wudl and A. L. Briseno, *J. Mater. Chem. C*, 2014, **2**, 3361-3366.
35 X. Gu, X. Xu, H. Li, Z. Liu and Q. Miao, *J. Am. Chem. Soc.*, 2015, **137**, 16203-16208.
36 J. Liu, S. Osella, J. Ma, R. Berger, D. Beljonne, D. Schollmeyer, X. Feng and K. Müllen, *J. Am. Chem. Soc.*, 2016, **138**, 8364-8367.
37 Y. S. Park, D. J. Dibble, J. Kim, R. C. Lopez, E. Vargas and A. A. Gorodetsky, *Angew. Chem. Int. Ed.*, 2016, **55**, 3352-3355.
38 M. Kawamura, E. Tsurumaki and S. Toyota, *Synthesis*, 2018, **50**, 134-138.
39 X.-S. Zhang, Y.-Y. Huang, J. Zhang, W. Meng, Q. Peng, R. Kong, Z. Xiao, J. Liu, M. Huang, Y. Yi, L. Chen, Q. Fan, G. Lin, Z. Liu, G. Zhang, L. Jiang and D. Zhang, *Angew. Chem. Int. Ed.*, 2020, **59**, 3529-3533.
40 L. Ma, S. Wang, Y. Li, Q. Shi, W. Xie, H. Chen, X. Wang, W. Zhu, L. Jiang, R. Chen, Q. Peng and H. Huang, *CCS Chem.*, 2022, **4**, 3669-3676.
41 Z. Liu, L. Wang, Q. Deng, J. Zhu, J. Sun, H. Wang, H. Fu and J. Yao, *ACS Materials Lett.*, 2023, **5**, 3010-3016.
42 L. Wang, L. Lin, T.-S. Zhang, S. Guo, Z. Liu, M. Zhang, S. Wang, G. Cui, W.-H. Fang, J. Zhu, H. Fu and J. Yao, *CCS Chem.*, 2023, **5**, 2264-2276.
43 Z. Wu, C. L. Anderson, T.-S. Zhang, Y. Liu, H. Fu and L. Wang, *Chem. Sci.*, 2025, **16**, 13374-13381.
44 Z. Zhao, S. Wang, X. Shi, H. Fu and L. Wang, *Chem. Sci.*, 2025, **16**, 5565-5572.
45 I. Carmichael and G. L. Hug, *J. Phys. Chem. Ref. Data*, 1986, **15**, 1-250.

View Article Online
DOI: 10.1039/D5SC06978E

46 S. W. Eaton, S. A. Miller, E. A. Margulies, L. E. Shoer, R. D. Schaller and M. R. Wasielewski, *J. Phys. Chem. A*, 2015, **119**, 4151-4161.

View Article Online
DOI: 10.1039/D5SC06978E

Data availability statements

The data supporting this article have been included as part of the Supplementary Information.